

The Radio Signatures of the First Supernovae

Avery Meiksin¹, Daniel J. Whalen²

*SUPA**, ¹*Institute for Astronomy, University of Edinburgh, Blackford Hill, Edinburgh EH9 3HJ, UK*

²*McWilliams Fellow, Department of Physics, Carnegie-Mellon University, Pittsburgh, PA 15213, USA*

30 November 2021

ABSTRACT

Primordial stars are key to primeval structure formation as the first stellar components of primeval galaxies, the sources of cosmic chemical enrichment and likely cosmic reionization, and they possibly gave rise to the super-massive black holes residing at the centres of galaxies today. While the direct detection of individual Pop III stars will likely remain beyond reach for decades to come, we show their supernova remnants may soon be detectable in the radio. We calculate radio synchrotron signatures between 0.5 – 35 GHz from hydrodynamical computations of the supernova remnants of Pop III stars in $\sim 10^7 M_\odot$ minihaloes. We find that hypernovae yield the brightest systems, with observed radio fluxes as high as 1 – 10 μJy . Less energetic Type II supernovae yield remnants about a factor of 30 dimmer and pair-instability supernova remnants are dimmer by a factor of more than 10,000. Because of the high gas densities of the progenitor environments, synchrotron losses severely limit the maximum emission frequencies, producing a distinctive peaked radio spectrum distinguishable from normal galactic supernova remnant spectra. Hypernovae radio remnants should be detectable by existing radio facilities like eVLA and eMERLIN while Type II supernova remnants will require the Square Kilometre Array. The number counts of hypernova remnants at $z > 20$ with fluxes above 1 μJy are expected to be one per hundred square degree field, increasing to a few per square degree if they form down to $z = 10$. The detection of a $z > 20$ Type II supernova remnant brighter than 1 nJy would require a 100–200 square degree field, although only a 1–2 square degree field for those forming down to $z = 10$. Hypernova and Type II supernova remnants are easily separated from one another by their light curves, which will enable future surveys to use them to constrain the initial mass function of Pop III stars.

Key words: radiation mechanisms: non-thermal – supernovae: general – galaxies: formation – cosmology: theory – radio continuum: galaxies

1 INTRODUCTION

The cosmic Dark Ages ended with the formation of the first stars in $10^5 - 10^6 M_\odot$ cosmological haloes at $z \sim 20 - 30$. Primordial (or Pop III) stars are the key to understanding primeval galaxies, the onset of early cosmological reionization and chemical enrichment, and the origins of the supermassive black holes found in most massive galaxies today. Unfortunately, in spite of their extreme luminosities (Schaerer 2002) and the arrival of next-generation near infrared (NIR) observatories such as the *James Webb Space Telescope* (*JWST*) and the Thirty-Meter Telescope (TMT), individual Pop III stars will remain beyond the reach of direct detection for decades to come. For now, there are no observational constraints on either their masses or their rates of formation.

On the simulation frontier, there has been a gradual shift in paradigm over the past decade from single 30 – 300 M_\odot stars forming in isolation in haloes (Bromm et al. 2002; Nakamura & Umemura 2001; Abel et al. 2002; O’Shea & Norman 2007, 2008; Wise & Abel 2007) to binaries (Turk et al. 2009) and more recently to the possibility of 20 – 40 M_\odot stars forming in small multiples of up to a dozen (Stacy et al. 2010; Clark et al. 2011; Greif et al. 2011; Hosokawa et al. 2011; Stacy et al. 2011; Greif et al. 2012). However, these simulations do not estimate Pop III stellar masses by modeling the formation and evolution of the stars. Instead, they usually derive them by comparing infall rates at the center of the halo at very early stages of collapse to Kelvin-Helmholz contraction times to place upper limits on the final mass of the star. No simulation currently bridges the gap between the initial formation and fragmentation of a protostellar disk and its photoevaporation up to a million years later, so

* Scottish Universities Physics Alliance

there are no firm numerical constraints on the Pop III IMF either. (See Whalen 2012, for a recent review of primordial star formation.)

Pop III stars profoundly transformed the haloes that gave birth to them, driving out most of their baryons in supersonic ionized outflows (Whalen et al. 2004; Kitayama et al. 2004; Alvarez et al. 2006; Abel et al. 2007) and later exploding as supernovae (SNe) (Bromm et al. 2003; Kitayama & Yoshida 2005; Greif et al. 2007; Whalen et al. 2008). Ionization fronts from these stars also engulfed nearby haloes, either promoting or suppressing star formation in them and regulating the rise of the first stellar populations (e.g. Shapiro et al. 2004; Iliev et al. 2005; Susa & Umemura 2006; Whalen et al. 2008; Hasegawa et al. 2009; Susa et al. 2009; Whalen et al. 2010). As each halo hosted consecutive cycles of stellar birth, H II region formation and SN explosions (Yoshida et al. 2007), gravity and accretion flows congregated them into the first primitive galaxies with halo merger time-scales of ~ 20 Myr at $z \sim 20$ (e.g. Johnson et al. 2008; Greif et al. 2008, 2010; Wise et al. 2012). At the same time, the first SNe enriched the IGM with metals and dust, triggering a transition from Pop III to Pop II star formation (e.g. Mackey et al. 2003; Smith & Sigurdsson 2007; Smith et al. 2009; Nagakura et al. 2009; Chiaki et al. 2012). How these two processes determined the masses and formation rates of stars in primeval galaxies at $z \sim 10 - 15$, and therefore their spectra and luminosities, is unknown.

Stellar evolution models show that the final fates of the first stars rested upon their masses at birth (Heger & Woosley 2002): $15 - 40 M_{\odot}$ Pop III stars died in core-collapse SNe (Joggerst et al. 2010) and $40 - 140 M_{\odot}$ stars collapsed to black holes, perhaps with violent pulsational mass loss prior to death (Woosley et al. 2007). Pop III stars from 140 to $260 M_{\odot}$ died as pair instability (PI) SNe, extremely energetic thermonuclear explosions with energies of up to 100 those of Type Ia and Type II SNe (Joggerst & Whalen 2011; Chatzopoulos & Wheeler 2012 extend this lower limit down to $65 M_{\odot}$ for rotating stars). Some $40 - 60 M_{\odot}$ Pop III stars may have died as hypernovae, with energies intermediate to those of core-collapse and PI SNe (Iwamoto et al. 2005). Attempts have been made to indirectly constrain the masses of the first stars by reconciling the cumulative nucleosynthetic yield of their supernovae to the chemical abundances found in ancient, dim metal-poor stars in the Galactic halo (Beers & Christlieb 2005; Frebel et al. 2005), some of which may be contaminated with the ashes of the first generation. For example, Joggerst et al. (2010) recently discovered that the average yields of $15 - 40 M_{\odot}$ Pop III SNe agree well with the fossil abundances measured in ~ 130 stars with metallicities $Z < 10^{-4} Z_{\odot}$ (Cayrel et al. 2004; Lai et al. 2008), suggesting that low-mass primordial stars may have synthesized most metals at high redshift. However, stellar archaeology is still in its infancy because of small sample sizes, systematics in the measurements of some elements, and because the imprint of metals from first-generation stars on the second is not well understood.

The direct detection of Pop III SNe may be the best prospect for probing the earliest generation of stars in the near term. Primordial supernovae may be 100,000 times brighter than their progenitors, or, at slightly lower red-

shifts, the primitive galaxies in which they reside. Their transience readily distinguishes them from early galaxies, with which they otherwise overlap in colour-colour space. Previous studies have investigated detection limits for PI SNe at $z \sim 6$ (Scannapieco et al. 2005; Tanaka et al. 2012), for $6 < z < 15$ (Pan et al. 2011; Moriya et al. 2012; Whalen et al. 2012, Whalen, Even et al. in preparation), and in very approximate terms for $z \sim 30$ (Hummel et al. 2012). Whalen, Fryer et al. (in preparation) and Whalen, Frey et al. (in preparation) show that *JWST* will detect PI SNe beyond $z \sim 30$ and that the *Wide Field Infrared Survey Telescope (WFIRST)* and the *Wide-field Imaging Surveyor for High-Redshift (WISH)* will detect them out to $z \sim 15 - 20$ in all-sky NIR surveys. Unfortunately, it may be a decade before such observations are possible, given that *JWST* and *WFIRST* will not be in operation before 2018 and 2021, respectively.

In the meantime, it may be possible to discover the first generation of supernovae in cosmic backgrounds. Pair instability SNe deposit up to half of their energy into the CMB via inverse Compton scattering at $z \sim 20$ (Kitayama & Yoshida 2005; Whalen et al. 2008). Oh et al. (2003) have found that Pop III PI SNe may impose excess power on the CMB on small scales via the Sunyayev-Zeldovich effect. Primordial SNe may also be manifest as fluctuations in the NIR background because they are so much more luminous than their host protogalaxies at high redshift.

In this paper, we show Pop III supernovae may also be revealed through the detection of the radio emission from their remnants by both current and future radio observatories such as the eVLA¹, eMERLIN², MeerKAT³, ASKAP⁴ and the Square Kilometre Array⁵ (SKA). A review of planned deep continuum radio surveys, including some that would be capable of detecting the remnants discussed here, is provided by Norris et al. (2012). Ioka & Mészáros (2005) previously suggested the radio afterglows of high redshift hypernovae would produce large fluxes while still relativistically expanding, however this phase is brief so that the probability of discovery of such systems in collapsing minihaloes is very low. The afterglows may be more common in primitive galaxies with established star formation.

Previous studies of the observability of collapsing structures at $z > 10$ in the radio have centered on detecting the 21cm signal of minihaloes during the cosmic dark ages (e.g. Furlanetto & Loeb 2002; Iliev et al. 2002; Shapiro et al. 2006; Meiksin 2011), not cosmic explosions at first light. There are several advantages to searching for the first supernovae through their radio synchrotron emission. Firstly, if only certain types of explosions contribute a radio signal, this may be used to place limits on the masses of their progenitors. Secondly, supernova (and hence star formation) rates may possibly be determined from the strength of the radio signals and the number counts of the sources. Finally, depending on the properties of this signal, it may be possible to pinpoint the redshift of the explosions.

In this paper we calculate the long term radio signal

¹ www.aoc.nrao.edu/evla/

² www.jb.man.ac.uk/research/rflabs/eMERLIN.html

³ public.ska.ac.za/meerkat

⁴ www.atnf.csiro.au/projects/askap

⁵ www.skatelescope.org

produced by the remnants of core-collapse SNe, hypernovae and PI SNe to assess the detectability of the remnants by current and future observatories. We also determine if this signal may constrain the masses and formation rates of Pop III stars in high redshift protogalaxies. In §2 we review how Pop III SN explosions generate synchrotron emission that could be directly detected by current and planned radio telescopes. In §3 we describe the expected radio light curves and number counts of the Pop III SN radio remnants. We summarise our conclusions in §4. Formulae are provided for synchrotron emission and self-absorption in terms of the energy densities of the relativistic electrons and the magnetic field in an appendix. The range in relativistic gamma factors is discussed in a second appendix.

For numerical cosmological estimates, we adopt $\Omega_m = 0.27$, $\Omega_v = 0.73$, $H_0 = 100h \text{ km s}^{-1} \text{ Mpc}^{-1}$ with $h = 0.70$, $\sigma_{8h^{-1}} = 0.81$ and $n = 0.96$ for the total mass and vacuum energy density parameters, the Hubble constant, the linear density fluctuation amplitude on a scale of $8h^{-1} \text{ Mpc}$ and the spectral index, respectively, consistent with the best-fitting cosmological parameters for a flat universe as constrained by the 5-yr *Wilkinson Microwave Anisotropy Probe* (*WMAP*) measurements of the Cosmic Microwave Background (Komatsu et al. 2009).

2 THE SYNCHROTRON SIGNATURE OF SUPERNOVAE IN MINI-HALOES

We begin by estimating the expected synchrotron flux from a supernova remnant. For relativistic electrons with energy density u_e in a magnetic field of energy density u_B , the bolometric emissivity of synchrotron radiation is

$$\epsilon_{\text{bol}} \sim u_e \tau_S^{-1}, \quad (1)$$

where τ_S is the characteristic synchrotron cooling time

$$\tau_S = \frac{3}{4} \frac{m_e c^2}{\sigma_T \gamma_u u_B}. \quad (2)$$

for the most energetic electrons with kinetic energy $(\gamma_u - 1)m_e c^2$, assuming $\gamma_u \gg 1$. Here σ_T is the Thomson cross section for electron scattering and m_e is the mass of an electron.

Allowing for a fraction f_e of the thermal energy to go into relativistic electrons, so that $u_e = f_e u_{\text{th}}$ for a thermal energy density u_{th} , and further assuming equipartition $u_B \simeq u_e$ (Chevalier 1982), the bolometric synchrotron power emitted by a single halo is

$$P_{\text{bol}}^{\text{sync}} \simeq 4\pi \gamma_u \frac{c \sigma_T}{m_e c^2} \int dr r^2 f_e(r)^2 u_{\text{th}}^2 F(p_e; \gamma_l, \gamma_u), \quad (3)$$

where the function $F(p_e; \gamma_l, \gamma_u)$, described in Appendix A, allows for a power-law energy distribution of index p_e for the relativistic electrons, and γ_l and γ_u are the lower and upper ranges of the relativistic γ factors for the electrons. The upper electron energies are generally believed to be due to acceleration within the region of the shock, although the precise mechanism is still unknown. Observations suggest values as high as $\gamma_u \simeq 10^8$ are achieved (Koyama et al. 1995). For the supernova remnants examined here, synchrotron cooling is sufficiently strong downstream of the shock that γ_u of a few hundred is more typical. A lower energy cut-off

γ_l is imposed by energy losses arising from the excitation of quantized plasma waves (plasmons). The computation of the range in relativistic electron energies used here is discussed in Appendix B.

The electron energy spectrum will generally evolve downstream of the shock due to synchrotron cooling, resulting in a steepening of the synchrotron spectrum above a break frequency around 100 GHz. The assumption of a constant f_e and p_e is therefore an approximation and should only be regarded as effective values. The model none the less qualitatively recovers the effects of the high frequency break, as discussed in Appendix B. The high frequency range of the spectrum, however, should be regarded as uncertain by factors of several.

We illustrate the expected flux using the computation for a $40 M_\odot$ hypernova in a $1.2 \times 10^7 M_\odot$ halo at $z = 17.3$ (Whalen et al. 2008). The synchrotron power may be estimated from the post-shock thermal energy density of the supernova remnant, which exceeds a few erg cm^{-3} over a region around a tenth of a parsec across during the first few years. For $f_e = 0.01$ (e.g. Chevalier 1982), this corresponds to a bolometric synchrotron power output of $P_{\text{bol}}^{\text{sync}} \simeq 5 \times 10^{42} \text{ erg s}^{-1}$ for $\gamma_u = 300$ and $p_e = 2$. The spectrum will extend to a lower characteristic cutoff wavelength, assuming an isotropic magnetic field, of $\lambda_c = (2\pi^{1/2}/3)(m_e c^2/e)\gamma_u^{-2}u_B^{-1/2} \simeq 2014\gamma_u^{-2}u_B^{-1/2} \text{ cm} \approx 0.2 \text{ cm}$, or upper cutoff frequency $\nu_c \simeq 130 \text{ GHz}$, corresponding to a characteristic specific power at ν_c of $2 \times 10^{31} \text{ erg s}^{-1} \text{ Hz}^{-1}$. For a source at $z = 17.3$, this corresponds to an observed radio flux of $\sim 10 \mu\text{Jy}$. The flux will vary with frequency as $\nu^{-(p_e-1)/2} = \nu^{-1/2}$.

The radio spectrum computed 4.7 yrs after the explosion is shown in Fig. 1. The thermal free-free radiation is shown as well, but is generally much smaller than the synchrotron. The energy density in relativistic electrons is sufficiently high that synchrotron self-absorption (SSA) is significant at the lower frequencies. Allowing for SSA severely attenuates the spectrum at $\nu \lesssim 40 \text{ GHz}$, as shown in Fig. 1.

Adding free-free absorption degrades the spectrum further at low frequencies. Free-free absorption was neglected from the fluid zone at the shock front, where the gas is becoming ionized but has not yet reached the post-shock temperature. Since the shock front is unresolved, the substantial free-free absorption from it is likely greatly over-estimated. For a shock front width on the order of the Coulomb mean free path, the free-free absorption from the shock front becomes negligible. It will therefore generally not be included here. It is remarked, however, that if cool circumstellar gas mixes in with the post-shock ionized gas, free-free absorption could be non-negligible. Such an effect is beyond the capacity of a spherically symmetric code to reproduce, and would be difficult to resolve in any case.

The Razin-Tsytovich plasma effect on the synchrotron radiation mechanism may further degrade the escaping synchrotron radiation (e.g. Scheuer & Williams 1968; Rybicki & Lightman 1986). We approximate the effect by cutting off the production of synchrotron radiation by the factor $\exp(-\nu_{\text{RT}}/\nu)$, where

$$\nu_{\text{RT}} = \gamma_u \nu_p \left(1 + \gamma_u \frac{\nu_p}{\nu_c} \right), \quad (4)$$

and ν_p is the electron plasma frequency. This strongly cuts

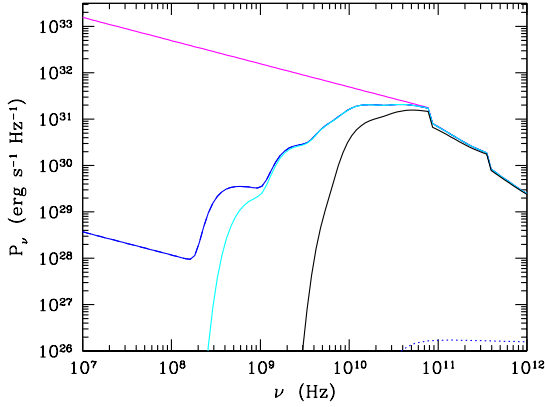


Figure 1. Radio power from a $40 M_{\odot}$ hypernova in a $1.2 \times 10^7 M_{\odot}$ minihalo at $z = 17.3$ (for $f_e = 0.01$ and $p_e = 2$). Shown are total (synchrotron and thermal free-free) (solid lines) and thermal free-free (dotted line) powers. The upper curve (magenta) corresponds to a model with no attenuation. The middle curves allow for synchrotron self-absorption (blue) and free-free absorption as well (cyan). The lowest curve (black) further adds hypothesized plasma synchrotron attenuation effects.

off most of the radiation below $\sim 0.1\nu_c$, as shown in Fig. 1. As the occurrence of the hypothesized effect is unclear, we conservatively neglect it further here except as noted, but remark that the detection of such greatly diminished low-frequency emission would support its reality.

Radio observations of supernova remnants do not strongly constrain f_e , although values of $f_e \sim 0.001 - 0.2$ are indicated (Weiler et al. 1986; Chevalier 1998; Soderberg et al. 2006). Assuming equipartition, the power at $\nu = \nu_c$ is proportional to $f_e^{3/2}$. It is worth noting that for $f_e \ll 1$, an equipartition magnetic field will contribute negligibly to the pressure forces acting on the post-shock gas, so that the hydrodynamical models used should not be much affected.

3 OBSERVATIONAL PREDICTIONS

Deep radio surveys are currently able to reach the few μJy level. The Very Large Array has achieved an *rms* noise level of $1.5 \mu\text{Jy}$ at 8.4 GHz (Fomalont et al. 2002) and $2.7 \mu\text{Jy}$ at 1.4 GHz (Owen & Morrison 2008). Similar levels have been reached using eMERLIN (Muxlow et al. 2005). The Square Kilometre Array is projected to be a factor 100–1000 more sensitive.

In Figs 2 and 3, we show the light curves for a $40 M_{\odot}$ hypernova and $15 M_{\odot}$ Type II supernova, respectively, in a $1.2 \times 10^7 M_{\odot}$ minihalo at $z = 17.3$ in the observed frame for selected bands planned for the SKA. The bands lie within the eVLA frequency range. The eMERLIN L-band includes 1.4 GHz, while the C-band flux light curve would lie between

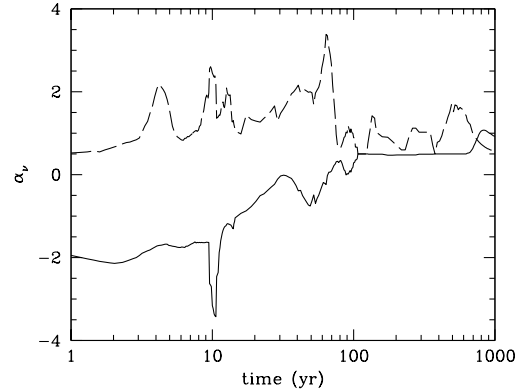
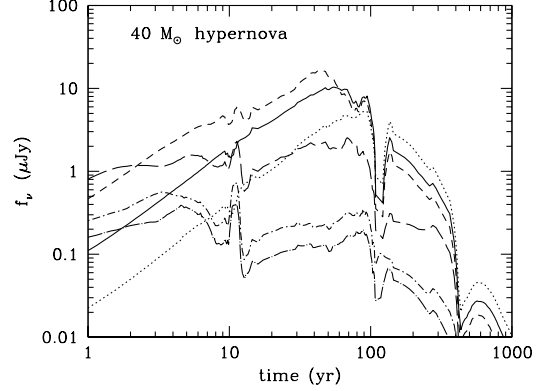


Figure 2. Top panel: Radio light curves for a $40 M_{\odot}$ hypernova in a $1.2 \times 10^7 M_{\odot}$ minihalo at $z = 17.3$ (for $p_e = 2$ and $f_e = 0.01$). The curves correspond to the bands: 0.5 (dotted), 1.4 (solid), 3 (short-dashed), 10 (long-dashed), 25 (dot short-dashed) and 35 (dot long-dashed) GHz. Bottom panel: The corresponding spectral indices at 1.4 (solid) and 10 (long-dashed) GHz.

those for the 3 and 10 GHz bands. For the $40 M_{\odot}$ hypernova, time-dilation produces a gradual rise in the observed flux f_{ν} extended over a 100 yr time-scale with an even slower decline. A flux exceeding $1 \mu\text{Jy}$ is expected to persist over a span of 300 yrs, with a peak flux of $\sim 10 \mu\text{Jy}$. Most notable is the relatively late rise of the flux in the 500 MHz band; it eventually overtakes the higher frequency fluxes for a period of 150 yrs while above $1 \mu\text{Jy}$.

Sizable fluctuations in the flux over time are found. These arise because the dominant emitting region lies just downstream of the shock front with a width governed by synchrotron and plasmon excitation losses, as described in Ap-

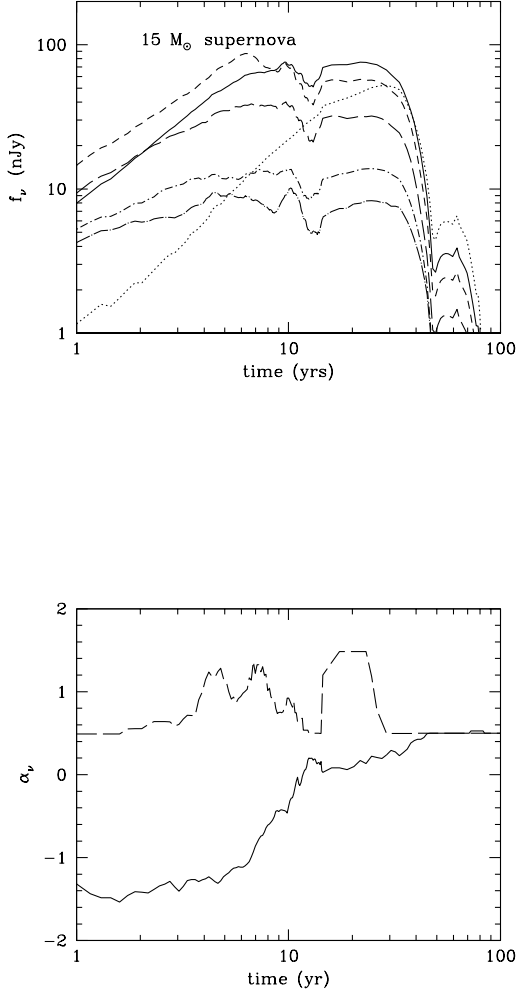


Figure 3. Top panel: Radio light curves for a $15 M_{\odot}$ Type II supernova in a $1.2 \times 10^7 M_{\odot}$ minihalo at $z = 17.3$ (for $p_e = 2$ and $f_e = 0.01$). The curves correspond to the bands: 0.5 (dotted), 1.4 (solid), 3 (short-dashed), 10 (long-dashed), 25 (dot short-dashed) and 35 (dot long-dashed) GHz. Bottom panel: The corresponding spectral indices at 1.4 (solid) and 10 (long-dashed) GHz.

pendix B. The width increases with decreasing gas density and magnetic field strength and decreases with decreasing shock velocity. As the shock slows and weakens, these factors work against each other, producing a fluctuating volume of emitting gas. For intermittent periods, the energy losses deplete the relativistic electron population except very near the shock front.

Since radio observations are often quantified by the spectral index $\alpha_{\nu} = -d \log f_{\nu} / d \log \nu$, the spectral indices at two representative SKA bands are shown in the lower panel. The changing structure of the post-shock gas produces varying spectral indices in the period leading up to

the peak emission. The low frequency attenuation results in $\alpha_{\nu} < 0$ at frequencies below 3 GHz. At late times, after the peak emission, the emission is dominated by a restricted region downstream of the shock front for which $\gamma_u > 1000$, and the spectral index at the lower frequencies settles to $\alpha_{\nu} = 0.5$, the value expected for a power-law relativistic electron energy distribution with $p_e = 2$.

Similar trends are found for the $15 M_{\odot}$ supernova, although over the much shorter time-scale of decades and with flux values lower by a factor of ~ 100 . We also computed the emission following a $260 M_{\odot}$ pair instability supernova, but found it so efficiently sweeps through the minihalo that the resulting observed radio flux is at most ~ 0.1 nJy. Similarly, we found the observed radio fluxes from the remnants produced in a $2 \times 10^6 M_{\odot}$ halo by all three supernova progenitor masses fell well below 1 nJy.

Allowing for the Razin-Tsytovich effect much reduces the flux in the 500 MHz band, as shown in Fig. 4. While it continues to rise with time, it lies about 1 dex below the flux at 1.4 GHz for 50 yrs, and never overtakes it. Comparison with Fig. 2 suggests the measured flux in the 500 MHz band may be used to detect the presence of the Razin-Tsytovich effect. The spectrum at 500 MHz is very steep, with $\alpha_{\nu} < -2.5$ during the first 100 yrs.

The number of sources visible per year is substantial. We estimate this from the halo collapse rate using the halo fitting function of Reed et al. (2007), adapted to the 5 yr *WMAP* cosmological parameters for a flat universe (Komatsu et al. 2009). The observed formation rate of haloes within a solid angle $\delta\Omega$ with a comoving number density $n_h^{\text{com}}(z)$ for halo masses exceeding M_h , integrated over $z_1 < z < z_2$, is then

$$\begin{aligned}
 \dot{N}_h^{\text{obs}}(> M_h) &= \int_{z_1}^{z_2} dz \dot{n}_h^{\text{com}}(1+z)^3 \frac{dV^{\text{prop}}}{dz} \frac{1}{1+z} \\
 &= - \int_{z_1}^{z_2} dz \frac{dn_h^{\text{com}}}{dz} c(a_0 r)^2 \delta\Omega \\
 &= [n_h^{\text{com}} c(a_0 r)^2]_{z_2}^{z_1} \delta\Omega \\
 &\quad + 2 \left(\frac{c}{H_0} \right) \int_{z_1}^{z_2} dz n_h^{\text{com}} c \frac{a_0 r}{[\Omega_m(1+z)^3 + \Omega_v]^{1/2}} \delta\Omega \\
 &\simeq n_h^{\text{com}}(z_1) c [a_0 r(z_1)]^2 \delta\Omega,
 \end{aligned} \tag{5}$$

where $a_0 r(z) = (c/H_0) \int_0^z dz [\Omega_m(1+z)^3 + \Omega_v]^{-1/2}$ is the angular size distance for a flat universe with present day mass and vacuum energy density parameters Ω_m and Ω_v , respectively, and Hubble constant H_0 . For $z_1 > 3$, $(H_0/c) a_0 r(z_1) \simeq 1.5 + 1.9[1 - 2/(1+z_1)^{1/2}]$ to better than 2 percent accuracy. The approximation $\dot{n}_h^{\text{com}} = (dn_h^{\text{com}}/dz)(dz/dt)$ was made, although this could be modified by allowing for merger histories. In the final line, the integral in the line previous was neglected as was the halo density at $z = z_2$. A factor $1/(1+z)$ has been included to account for time-dilation.

We find formation rates for haloes $M > 10^7 h^{-1} M_{\odot}$ and $z > 20$ of $0.0016 \text{ deg}^{-2} \text{ yr}^{-1}$, and $0.20 \text{ deg}^{-2} \text{ yr}^{-1}$ at $z > 10$. These amount to about 70 to 8000 collapsing haloes per year over the sky. The rates are comparable to recent predictions for the total production rate of Pop III pair instability supernovae, with progenitor masses between $140 - 260 M_{\odot}$, based on cosmological simulations (e.g. Hummel et al. 2012; Johnson et al. 2012), assuming one PI SN per minihalo formed. On the other hand, small scale simulations suggest

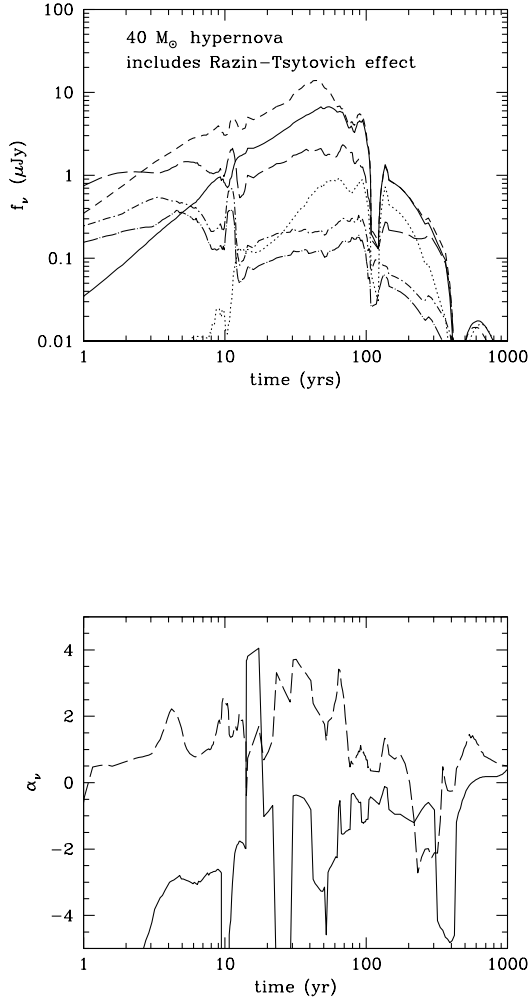


Figure 4. Top panel: Radio light curves for a $40 M_{\odot}$ hypernova in a $1.2 \times 10^7 M_{\odot}$ minihalo at $z = 17.3$ (for $p_e = 2$ and $f_e = 0.01$). The Razin-Tsytoich effect is included. The curves correspond to the bands: 0.5 (dotted), 1.4 (solid), 3 (short-dashed), 10 (long-dashed), 25 (dot short-dashed) and 35 (dot long-dashed) GHz. Bottom panel: The corresponding spectral indices at 1.4 (solid) and 10 (long-dashed) GHz.

fragmentation may prevent the formation of Pop III stars sufficiently massive to form a PI SN (e.g. Stacy et al. 2010), although subsequent mergers of the protostars into more massive ones cannot be ruled out. The star formation may also be stochastic given the low number of massive stars formed, with hypernovae forming before a more massive PI SN progenitor is created.

The effect of multiple supernovae on the gas in small haloes is unknown. The heat input of a supernova is sufficient to unbind the IGM of a minihalo with mass below $\sim 10^7 M_{\odot}$, while, once the gas cools, it will fall back in a

more massive system (Whalen et al. 2008; Meiksin 2011). The remaining massive stars will further replenish the IGM through winds, so a gaseous environment may continue to persist on which further supernovae may impact, producing synchrotron emitting remnants. If each halo gives rise to at least one supernova with progenitor mass exceeding $40 M_{\odot}$, its remnant should then be detectable by eVLA or eMERLIN. If each produces one with a progenitor mass exceeding $15 M_{\odot}$, SKA should be able to detect the remnant.

An estimate of the expected number counts of radio emitting remnants requires modelling the remnants over a broad redshift range. In the absence of simulations covering a wide range, we use those discussed above, presuming the behaviour of the gas is not very sensitive to redshift. This is a coarse approximation, as the gas content of the haloes is expected to be sensitive to the redshift of their formation. On the other hand, since much of the gas into which the supernova explodes is produced by stellar winds, the environment of the progenitor may not be very redshift dependent. An improved estimate would require a better understanding of star formation within primordial haloes.

The number of sources with observed flux exceeding f_{ν} is given by modifying equation (5) to account for the duration $\delta t_{f_{\nu}}^{\text{eff}}(z)$ the remnant is visible with a flux exceeding f_{ν} :

$$N(> f_{\nu}) = - \int_{z_1}^{z_2} dz \frac{dn_h^{\text{com}}}{dz} c(a_0 r)^2 \delta t_{f_{\nu}}^{\text{eff}}(z) \delta \Omega. \quad (6)$$

The resulting number counts for haloes collapsing at $z > 20$ are shown in Fig. 5, based on one $40 M_{\odot}$ hypernova per collapsing halo with a mass exceeding $10^7 h^{-1} M_{\odot}$. In the lower frequency bands, the counts decline above $0.3 \mu\text{Jy}$ but are still substantial to $\sim 10 \mu\text{Jy}$. A source brighter than $1 \mu\text{Jy}$ should be visible in the range $0.5 < \nu < 3\text{GHz}$ every 100 square degrees.

Few young sources are found below $1 \mu\text{Jy}$. This is because at a rest-frame age of about 21 yrs, the width of the emitting region diminishes to about 10^{15} cm, resulting in very little emission (see Appendix B), and a plateau in the number counts. By an age of 32 yrs, as the shock further weakens, the emission zone broadens to about 3×10^{16} cm, and the flux somewhat recovers (as is visible in Fig. 2 after 400 yrs in the observed frame). This produces a rise in the number counts at very low flux levels, giving about one source brighter than 1nJy per 10 square degrees in the low frequency bands.

At the earliest epochs of star formation, although the remnants would still have observed peak fluxes brighter than $1 \mu\text{Jy}$, the frequency of their occurrence becomes very small. We find only one remnant at $z > 30$ brighter than 1nJy is expected over the entire sky.

Johnson et al. (2012) suggest Pop III star formation may persist to $z < 10$. This substantially boosts the counts to a few per square degree brighter than $1 \mu\text{Jy}$, and more than 10 per square degree brighter than 1nJy . The sources may be identified by the weakness of the 25 and 35 GHz fluxes compared with the lower frequency fluxes, a signature of strong synchrotron cooling, although the fluxes at these high frequencies are difficult to predict because of the effects of energy loss on the energy distribution of the relativistic electrons (see Appendix B). More definitive would be a survey campaign with repeat multiband observations extended

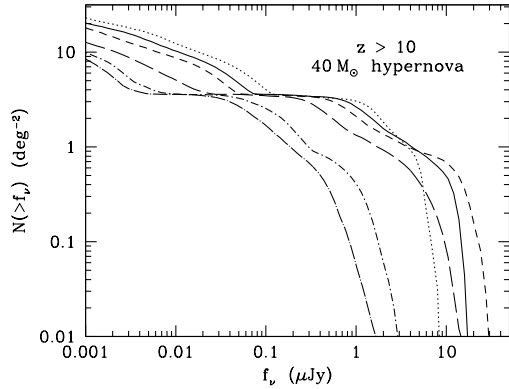
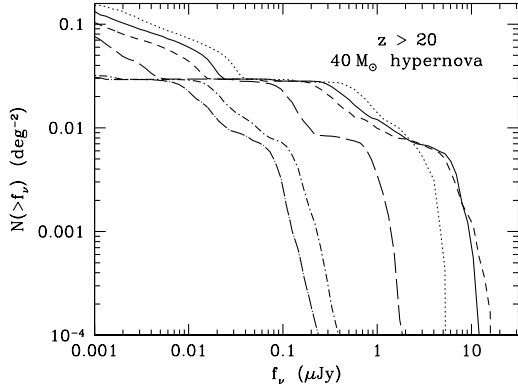


Figure 5. Number counts of radio remnants above a given flux, based on radio light curves for a $40 M_{\odot}$ hypernova in $1.2 \times 10^7 M_{\odot}$ minihaloes (for $p_e = 2$ and $f_e = 0.01$) at $z > 20$ (upper panel) and $z > 10$ (lower panel). The observed counts are shown for bands: 0.5 (dotted), 1.4 (solid), 3 (short-dashed), 10 (long-dashed), 25 (dot short-dashed) and 35 (dot long-dashed) GHz.

over several years to trace the light curves, especially during the early rising phase.

The corresponding number counts based on one $15 M_{\odot}$ Type II supernova per collapsing halo are shown in Fig. 6. While the fluxes are considerably weaker than for the more energetic hypernovae, the numbers are lower also as a result of their shorter durations. To detect the remnants at $z > 20$, 100–200 square degree fields would be required to detect remnants as weak as 1 nJy. The counts for $z > 10$ are considerably higher, requiring now 1–2 square degree fields to detect the supernova remnants at the 1 nJy level.

We have also examined the radio absorption signature

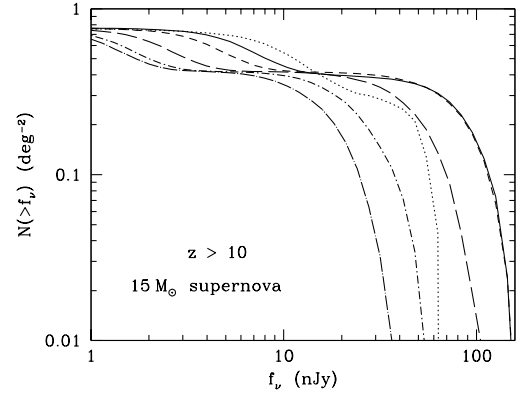
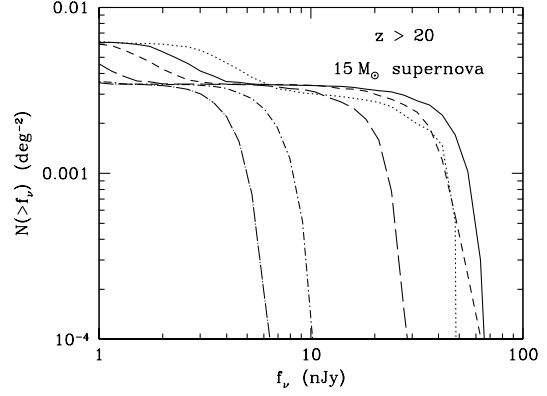


Figure 6. Number counts of radio remnants above a given flux, based on radio light curves for a $15 M_{\odot}$ Type II supernova in $1.2 \times 10^7 M_{\odot}$ minihaloes (for $p_e = 2$ and $f_e = 0.01$) at $z > 20$ (upper panel) and $z > 10$ (lower panel). The observed counts are shown for bands: 0.5 (dotted), 1.4 (solid), 3 (short-dashed), 10 (long-dashed), 25 (dot short-dashed) and 35 (dot long-dashed) GHz.

of the remnants against a bright background radio source. While synchrotron absorption will produce a strong absorption feature at rest frame frequencies below 20 GHz, it persists for less than ~ 100 yr. The number of detectable features along a line of sight will be

$$\frac{dN(> \tau_{\nu})}{dz} = n_h^{\text{com}} \pi (r_0^{\text{com}})^2 (1+z) c \delta t_{\tau_{\nu}}^{\text{eff}}(z), \quad (7)$$

where r_0^{com} is the comoving radius of the remnant out to which the line-of-sight absorption optical depth exceeds τ_{ν} and $\delta t_{\tau_{\nu}}^{\text{eff}}(z)$ is the effective duration of the feature. For a characteristic comoving radius of ~ 1 pc, $dN/dz \sim 3 \times 10^{-14}$

at $z = 10$, so that the feature would be undiscoverable. At late times, at $t \sim 0.8$ Myr, the outflowing gas cools sufficiently to produce a 21cm absorption feature that would be measurable by SKA. We find a characteristic 21cm absorption doublet arising from the cooling shell would form along lines of sight within ~ 5 pc (proper) of the centre of the minihalo. The feature would survive about 1 Myr before transforming into a singlet absorption feature indistinguishable from those expected from minihaloes. This corresponds to $dN/dz \sim 10^{-6}$, again too small to be discovered as there would still not be nearly an adequate number of bright background radio sources to have a fair chance of seeing even one feature.

4 CONCLUSIONS

We estimate the radio signatures of Pop III supernovae in $\sim 10^7 M_\odot$ minihaloes, sufficiently massive to retain their baryons and form supernova remnants, based on hydrodynamical computations of $15 M_\odot$ Type II supernovae, $40 M_\odot$ hypernovae and $260 M_\odot$ pair instability supernovae at $z = 17.3$ within the haloes. We model the synchrotron emission and absorption assuming a power-law distribution of relativistic electron energies with a total energy density proportional to the thermal energy of the ionized gas, and equipartition between the relativistic electron and magnetic field energies. Allowing for a relativistic electron component with total energy one to ten percent of the gas thermal energy is sufficient for a hypernova to produce observable fluxes at $0.5 - 10$ GHz exceeding $1 \mu\text{Jy}$ and for the less massive Type II supernova to produce observable fluxes exceeding 10 nJy at $0.5 - 25$ GHz.

The PI SN expels much of the halo gas, leaving behind a supernova remnant that produces fluxes of at most 0.1 nJy. A halo mass exceeding $10^8 h^{-1} M_\odot$ would be sufficient to retain the baryons following a PI SN. Although we do not currently have computations of PI SN in such massive haloes, we may estimate the halo formation rates: $0.011 \text{ deg}^{-2} \text{ yr}^{-1}$ if forming at $z > 10$, and $9.1 \times 10^{-6} \text{ deg}^{-2} \text{ yr}^{-1}$ for those forming at $z > 20$. These are about a factor 20–200 smaller than the formation rates of minihaloes with masses exceeding $10^7 h^{-1} M_\odot$, but would still produce a detectable yield of PI SNe remnants over the sky provided their synchrotron fluxes were sufficiently high.

Hypernovae at $z = 17.3$ produce observed light curves that rise gradually over a period of 100 yrs, and decline slowly over the subsequent 200–300 yrs. By contrast, the Type II curves have rise times of 5–10 yrs at frequencies above 1.4 GHz, and decline abruptly after another 30 yrs. The 500 MHz flux lags the higher frequency bands for both supernovae and dominates the emission shortly after it peaks as the synchrotron spectrum reddens due to the weakening of the supernova shock. Light curves computed with and without the hypothesized Razin-Tsytoich effect show that the observed 500 MHz flux is substantially diminished by the effect, suggesting it may provide a useful means of testing for the presence of the effect.

The light curves for both the hypernova and Type II supernova remnants in collapsing minihaloes may be distinguished from their galactic counterparts by the weakness of their high frequency fluxes. The flux decreases be-

low the power-law prediction at rest-frame frequencies above 100 GHz as a consequence of intense synchrotron cooling downstream of the shock front in the high gas density environments of the minihaloes, curtailing the maximum synchrotron frequency. Predictions of the precise shape of the high frequency spectrum, however, are complicated by the transport of relativistic electrons in the presence of strong synchrotron and plasmon excitation energy losses and the unknown magnetic field distribution.

Estimating the number counts of the supernovae from the minihalo formation rate at $z > 20$, we find a supernova formation rate of about one per 600 square degrees per year. If the supernovae are able to form down to $z = 10$, the rate increases to one per 5 square degrees per year. On average, one $z > 20$ hypernova radio remnant with flux exceeding $1 \mu\text{Jy}$ should be detectable at any given time per 100 square degree field, and one with a flux above 1 nJy per 10 square degree field. If Pop III star formation persists to $z < 10$, then a few hypernova remnants brighter than $1 \mu\text{Jy}$ would be visible per square degree, and more than ten per square degree brighter than 1 nJy.

Because of their smaller explosion energies, Type II supernovae will produce weaker radio remnants with shorter durations. Fields of 100–200 square degrees would be required to detect remnants forming at $z > 20$ with fluxes above 1 nJy. The numbers are much improved for supernovae forming down to $z < 10$, requiring instead 1–2 square degree fields to detect their radio remnants.

Pop III supernova remnants with radio fluxes exceeding $1 \mu\text{Jy}$ should be visible in radio surveys using the eVLA or eMERLIN, or possibly the MIGHTEE survey conducted with the SKA pathfinder MeerKAT. Weaker few nJy sources would be detectable by the SKA in large numbers. An observing campaign extended over several years would be able to follow the light curves, yielding invaluable data on the formation of the first stars in the Universe and their impact on their local environments.

The readily distinguishable differences between the radio light curves of hypernova and Type II supernova remnants provide the possibility of exploiting the radio emission to infer the initial mass function of the first stars. The frequency with which these explosions are detected over the sky will also constrain Pop III star formation rates through cosmic time along with all-sky NIR surveys by *WFIRST* and *WISH* and deep-field surveys by *JWST*. Their discovery in the radio will permit followup by deep-field observations of the host galaxies by *JWST* and the TMT. Surveys detecting Pop III radio remnants at $10 < z < 15$ may also constrain the multiplicity of their occurrence within individual primeval galaxies, and even the large-scale distribution of the galaxies themselves. The detection of primordial supernova remnants promises to be one of the most spectacular discoveries in high-redshift radio astronomy over the coming decade.

APPENDIX A: SYNCHROTRON EMISSION AND ABSORPTION

The synchrotron emissivity for a power-law relativistic electron energy distribution $dN/d\gamma \sim \gamma^{-p_e}$ extending over the

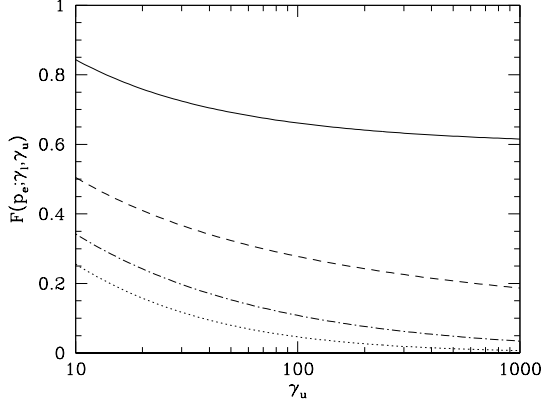


Figure A1. Synchrotron function $F(p_e; \gamma_l, \gamma_u)$ for relativistic electron power-law energy distribution over $\gamma_l < \gamma < \gamma_u$ with index p_e . Shown for $p_e = 1.5$ (solid line), $p_e = 2.0$ (dashed line), $p_e = 2.5$ (dot-dashed line) and $p_e = 3.0$ (dotted line). (A value $\gamma_l = 1$ is adopted.)

γ factor range $\gamma_l < \gamma < \gamma_u$ may be expressed concisely as

$$\epsilon_\nu = \begin{cases} \frac{3-p_e}{2} \frac{\epsilon_{\text{bol}}}{\nu_c} \left(\frac{\nu}{\nu_c}\right)^{-\frac{p_e-1}{2}} & ; \frac{1}{3} < p_e < 3 \\ \frac{1}{\log(\nu_c/\nu_{\text{min}})} \frac{\epsilon_{\text{bol}}}{\nu_c} \left(\frac{\nu}{\nu_c}\right)^{-1} & ; p_e = 3, \end{cases} \quad (\text{A1})$$

where ν_c is the synchrotron upper cutoff frequency

$$\nu_c = \frac{3}{4\pi} \frac{\gamma_u^2 e B \sin \alpha}{m_e c} \quad (\text{A2})$$

for pitch angle α , and ϵ_{bol} is the bolometric emissivity

$$\epsilon_{\text{bol}} = \frac{3}{4} u_e \tau_S^{-1} F(p_e; \gamma_l, \gamma_u). \quad (\text{A3})$$

Here, u_B is the energy density of the magnetic field, the synchrotron cooling time τ_S is given by equation (2) and the function $F(p_e; \gamma_l, \gamma_u)$, shown in Fig. A1, is

$$F(p_e; \gamma_l, \gamma_u) = 3^{1/2} \frac{9}{4\pi} \frac{2^{(p_e-1)/2}}{p_e+1} \Gamma\left(\frac{p_e}{4} + \frac{19}{12}\right) \Gamma\left(\frac{p_e}{4} - \frac{1}{12}\right) \times \begin{cases} \frac{2-p_e}{3-p_e} \frac{1-(\gamma_l/\gamma_u)^{3-p_e}}{1-(\gamma_l/\gamma_u)^{2-p_e}} & ; p_e \neq 2, p_e \neq 3 \\ \frac{1-\gamma_l/\gamma_u}{\log(\gamma_u/\gamma_l)} & ; p_e = 2 \\ \frac{\log(\gamma_u/\gamma_l)}{\gamma_u/\gamma_l - 1} & ; p_e = 3. \end{cases} \quad (\text{A4})$$

The inverse attenuation length due to synchrotron self-absorption may be expressed as

$$\alpha_\nu = r_0^{-1} \left(\frac{1}{\nu_c \tau_{\text{se}}}\right) \left(\frac{\nu_c}{\nu}\right)^{(p_e+4)/2} G(p_e; \gamma_l, \gamma_u), \quad (\text{A5})$$

where r_0 is the classical electron radius, $\tau_{\text{se}} = \gamma_u m_e c^2 / c \sigma_T u_e$

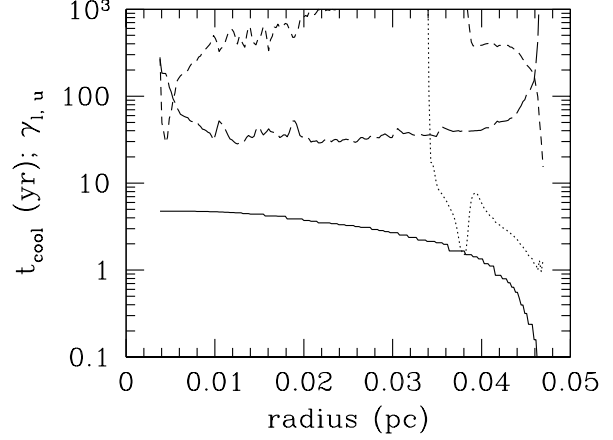


Figure B1. The time since shock passage (solid line) and the non-thermal bremsstrahlung cooling time (dotted line) for electrons with relativistic γ_u factor (long dashed line) corresponding to the synchrotron cooling time matching the time since shock passage. Also shown is the lower limiting γ_l factor (short dashed line) below which electrons lose energy to plasmon excitation on a time scale shorter than shock passage. Emission is dominated by the layers immediately downstream of the shock front at 0.047 pc. Shown for a $40 M_\odot$ hypernova 4.8 yr after the explosion, with $f_e = 0.01$, $u_B = u_e$ and $p_e = 2.0$ assumed.

is the characteristic electron scattering time, and

$$G(p_e; \gamma_l, \gamma_u) = \frac{3^{1/2}}{16\pi} \frac{2^{p_e/2}}{\gamma_u^3} \Gamma\left(\frac{p_e}{4} + \frac{1}{6}\right) \Gamma\left(\frac{p_e}{4} + \frac{11}{6}\right) \times \begin{cases} \frac{2-p_e}{1-(\gamma_l/\gamma_u)^{2-p_e}} & ; p_e \neq 2 \\ \frac{1}{\log(\gamma_u/\gamma_l)} & ; p_e = 2. \end{cases} \quad (\text{A6})$$

APPENDIX B: RANGE IN RELATIVISTIC ELECTRON ENERGIES

The dominant energy loss processes of relativistic electrons in the supernova remnants examined are synchrotron cooling, bremsstrahlung losses through scattering off the background thermal distribution of ions, and the excitation of plasmon waves. We discuss each of these in turn, using the rate estimates from Gould (1975).

No definitive acceleration mechanism for non-thermal relativistic electrons in supernova remnants has been identified, although mechanisms involving the diffusive acceleration of particles by shock waves, a form of first-order Fermi acceleration, are favoured. The characteristic acceleration time, assuming Bohm diffusion, is

$$t_{\text{acc}} \simeq \frac{r_g c}{u_{\text{sh}}^2}, \quad (\text{B1})$$

where $r_g = \gamma m_e c^2 / eB \simeq 1700(\gamma/B)$ cm is the gyroradius of an electron with relativistic velocity factor γ in a magnetic field B , and u_{sh} is the shock velocity (Malkov & O'C Drury

2001). Requiring the acceleration time to be shorter than the synchrotron cooling time (equation [2]) imposes the upper limit

$$\gamma_u^{(\text{sync})} < 1.2 \times 10^6 B^{-1/2} \left(\frac{u_{\text{sh}}/c}{0.01} \right), \quad (\text{B2})$$

corresponding to a limiting electron energy of ~ 1 TeV.

Downstream from the shock, at distances sufficiently far from the shock front the electrons are not rapidly returned by turbulent eddies, the electrons will cool in the absence of any other accelerating mechanism. At a time $t^{\text{p-sh}}$ after a shock, synchrotron cooling will result in

$$\gamma_u^{(\text{p-sh, sync})} < 77.4 B^{-2} \left[\frac{t^{(\text{p-sh})}}{10^7 \text{ s}} \right]^{-1}. \quad (\text{B3})$$

The electrons will also lose energy through scatters off other electrons and the ions, generating non-thermal bremsstrahlung radiation. The resulting cooling time is given by

$$(t_{\text{cool}}^{\text{n-th brems}})^{-1} = \frac{3}{\pi} \alpha \sigma_T c (n_{\text{H}} + 3n_{\text{He}}) \left[\log(2\gamma) - \frac{1}{3} \right], \quad (\text{B4})$$

where α is the fine structure constant. Requiring $t_{\text{cool}}^{\text{n-th brems}} > t_{\text{accel}}$ imposes

$$\gamma_u^{(\text{n-th-b})} < 4 \times 10^{10} \left(\frac{n_{\text{H}}}{10^7 \text{ cm}^{-3}} \right)^{-1} \left(\frac{u_{\text{sh}}/c}{0.01} \right)^2 B, \quad (\text{B5})$$

a less stringent constraint than given by synchrotron cooling for $B > 0.001 \{ (n_{\text{H}}/10^7 \text{ cm}^{-3}) [0.01/(u_{\text{sh}}/c)] \}^{2/3}$ G. For γ factors of order 100, the non-thermal bremsstrahlung cooling time approaches the synchrotron cooling time.

Relativistic electrons will also lose energy through plasmon excitation. The associated cooling time is

$$\begin{aligned} (t_{\text{cool}}^{\text{e-pl}})^{-1} &= \frac{3}{2} \sigma_T n_e c \gamma^{-1} \left[\log \left(\gamma^{1/2} \frac{m_e c^2}{h \nu_p} \right) + 0.216 \right] \\ &\simeq 2.99 \times 10^{-7} \frac{n_e}{10^7 \text{ cm}^{-3}} \gamma^{-1} \\ &\times \left[(1/2) \log \left(1.89 \times 10^{25} \frac{10^7 \text{ cm}^{-3}}{n_e} \gamma \right) + 0.216 \right] \text{ s}^{-1}. \end{aligned} \quad (\text{B6})$$

In this case, the lowest energy electrons cool most quickly. Generally $t_{\text{cool}}^{\text{e-pl}} \gg t_{\text{acc}}$ for the supernova remnants considered. The requirement $t_{\text{cool}}^{\text{e-pl}} > t^{\text{p-sh}}$ imposes the lower limit on γ of

$$\gamma_l^{(\text{p-sh, e-pl})} \simeq 94.5 \left(\frac{n_e}{10^7 \text{ cm}^{-3}} \right) \left(\frac{t^{\text{p-sh}}}{10^7 \text{ s}} \right), \quad (\text{B7})$$

to within 5 percent accuracy for $t^{\text{p-sh}}$ within an order of magnitude of 10^7 s.

The upper limit in the relativistic γ factor for the electrons is restricted primarily by synchrotron cooling, as illustrated in Fig. B1 for a $40 M_{\odot}$ hypernova in a $1.2 \times 10^7 M_{\odot}$ halo at $z = 17.3$, assuming $f_e = 0.01$, $u_B = u_e$ and $p_e = 2.0$. Also shown are the upper and lower relativistic factors γ_u and γ_l given by equating the synchrotron cooling time and plasmon excitation energy loss time, respectively, to the time since shock passage. By comparison, cooling due to non-thermal bremsstrahlung losses is generally negligible. Most of the interior of the supernova remnant would deplete its relativistic electrons due to synchrotron and plasmon excitation losses. Almost all the emission originates in a thin layer just downstream of the shock

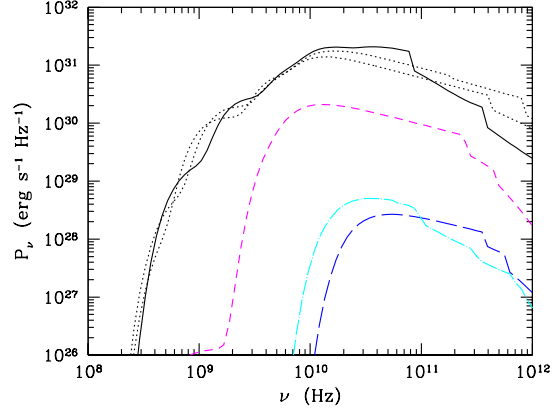


Figure B2. The evolution of the synchrotron emission spectrum allowing for synchrotron self-absorption and free-free absorption, with γ_l limited by loss to plasmon excitation and γ_u limited by synchrotron losses. Shown for a $40 M_{\odot}$ hypernova, with $f_e = 0.01$, $u_B = u_e$ and $p_e = 2.0$ assumed, at times 4.7 (solid; black), 17.4 (short-dashed; magenta), 21.4 (long dashed; blue) and 32.5 yrs (dot-dashed; cyan) after the explosion. Also shown are models at 4.7 yrs after the hypernova, allowing f_e to decrease due to cooling from an initial value of $f_e^i = 0.05$ with $u_B/u_{\text{therm}} = 0.05$ held fixed (upper dotted curve; black) and with the initial value of $f_e^i = 0.1$ and equipartition $u_B = u_e$ maintained (lower dotted curve; black).

front. The thickness Δl_{em} of the layer may be estimated by requiring $\gamma_l^{(\text{p-sh, e-pl})} < \gamma_u^{(\text{p-sh, sync})}$, giving $\Delta t_{\text{em}}/10^7 \text{ s} < 0.90 (n_e/10^7 \text{ cm}^{-3})^{-1/2} B^{-1}$, or

$$\Delta l_{\text{em}} = u_{\text{sh}} \Delta t_{\text{em}} < 2.7 \times 10^{15} \left(\frac{u_{\text{sh}}/c}{0.01} \right) \left(\frac{n_e}{10^7 \text{ cm}^{-3}} \right)^{-1/2} B^{-1} \text{ cm}. \quad (\text{B8})$$

Because of the steep rise in the thermal energy density just behind the shock front, the emission is not much increased by relaxing γ_l to unity.

The evolution of the spectrum for a $40 M_{\odot}$ hypernova remnant in a $1.2 \times 10^7 M_{\odot}$ minihalo is shown at $z = 17.3$ in Fig. B2 for $f_e = 0.01$ and $p_e = 2$, with γ_l and γ_u restricted by energy losses. The curve at the time 17.4 yrs corresponds to density and temperature profiles shown in Whalen et al. (2008). The emission power decays with time as the shock weakens and the emitting region reduces in width according to Eq. (B8). At 21.4 yrs after the hypernova, the emitting zone has narrowed to 10^{15} cm. By 32.5 yrs, however, the shock has weakened sufficiently for the emitting zone to broaden to 3×10^{16} cm, and the flux slightly recovers.

Because of energy losses by the relativistic electrons, a model with a constant value for f_e is an approximation. While the reduction in γ_u from synchrotron losses will little affect the total energy content in relativistic electrons for $p_e > 2$ because most of the energy is at the lower energy end of the spectrum, it will reduce the flux for $p_e < 2$. For

$p_e = 2$ the energy is logarithmically distributed. For an initial range $\gamma_i^i < \gamma < \gamma_u^i$, a final range $\gamma_l < \gamma < \gamma_u$ will retain a fraction $\log(\gamma_u/\gamma_l)/\log(\gamma_u^i/\gamma_i^i)$ of the original energy. For $\gamma_i^i = 1$, $\gamma_u^i = 10^6$, $\gamma_l = 50$, $\gamma_u = 300$, this gives a fraction 13% of the original energy. Thus an initial fraction $f_e^i = 0.1$ would be reduced to $f_e = 0.013$. Since the magnetic energy density would not directly be reduced by the losses, equipartition may not apply, in which case $u_B > u_e$ may be possible, depending on the time to establish equipartition. Spectra allowing for the energy loss since the time the gas was shocked are also shown in Fig. B2 at 4.7 yrs after the explosion for two alternative models, one assuming an initial post-shock value $f_e^i = 0.05$ and a post-shock magnetic energy density to thermal energy density ratio fixed at 0.05 and the second assuming an initial post-shock value $f_e^i = 0.1$ and a magnetic energy density that maintains equipartition with the evolving energy density of the relativistic electrons. Both these models well match the constant $f_e = 0.01$ model, so that the constant f_e model is a good approximation, noting that the value for f_e is effectively an average value.

At frequencies above ~ 100 GHz, the models allowing for an evolving f_e due to cooling show an enhanced flux over the constant effective f_e model in Fig. B2. In fact even in an evolving f_e model, the flux is expected to steepen at high frequencies due to synchrotron losses. Under the assumptions of a uniform shock velocity gas with a uniform magnetic field and diffusion coefficient independent of electron momentum, Heavens & Meisenheimer (1987) solve the steady-state transport equation for the population of relativistic electrons in the planar limit in the presence of strong synchrotron cooling. They show a power-law emission spectrum $\nu^{-0.5}$ will steepen to ν^{-1} above a break frequency ν_b before cutting off above the maximum frequency given by γ_u . The steepening is argued for on the general grounds that the distance over which electrons cool out of the distribution varies like γ^{-1} for synchrotron cooling. The break frequency depends on the specific model. They find $\nu_b \simeq 15 B^{-3} [(u_{sh}/c)/0.01]^2 (\Delta l_{em}/10^{15} \text{ cm})^{-2}$ GHz. For $B = 0.1$ G and $\Delta l_{em} = 10^{16}$ cm, this gives $\nu_b \simeq 150$ GHz. While the diffusion coefficient is generally expected to be proportional to the electron momentum (Malkov & O’C Drury 2001), the estimated break frequency is comparable to that at which the constant effective f_e model lies below the evolving f_e models and so may give a more realistic representation of the spectrum. A more precise prediction would require solving the relativistic electron transport equation, allowing for a non-uniform shock speed and magnetic field as well as a momentum-dependent diffusion coefficient; this is well beyond the scope of this paper, and the predicted synchrotron spectrum would in any case still depend on the assumed magnetic field properties and initial electron spectrum. In the absence of a definitive theory of relativistic electron acceleration and equipartition, the values $f_e = 0.01$ and $u_B = u_e$ are assumed for the estimates here, noting that these are only meant to represent effective values.

As indicated by the above discussion, the results computed in this paper will be quantitatively affected by several unknown factors, including the relativistic electron acceleration mechanism, the generation of turbulence at the shock front and its effects on the relativistic electron energy spectrum and possibly on the propagation of the shock front itself, and the subsequent transport of the relativistic elec-

trons as they cool due both to synchrotron and plasmon excitation losses. By scaling the uncertainties based on observed supernova remnants, we expect to minimize the effects of these uncertainties on our predictions, but naturally cannot eliminate them.

ACKNOWLEDGMENTS

We thank Philip Best, Jim Dunlop and Jeff Peterson for valuable discussions. We thank the referee for useful comments. DJW was supported by the Bruce and Astrid McWilliams Center for Cosmology at Carnegie Mellon University. All ZEUS-MP simulations were performed on Institutional Computing (IC) platforms at LANL (Coyote).

REFERENCES

- Abel T., Bryan G. L., Norman M. L., 2002, *Science*, 295, 93
- Abel T., Wise J. H., Bryan G. L., 2007, *ApJ*, 659, L87
- Alvarez M. A., Bromm V., Shapiro P. R., 2006, *ApJ*, 639, 621
- Beers T. C., Christlieb N., 2005, *ARA&A*, 43, 531
- Bromm V., Coppi P. S., Larson R. B., 2002, *ApJ*, 564, 23
- Bromm V., Yoshida N., Hernquist L., 2003, *ApJ*, 596, L135
- Cayrel R., Depagne E., Spite M., Hill V., Spite F., François P., Plez B., Beers T., Primas F., Andersen J., Barbuy B., Bonifacio P., Molaro P., Nordström B., 2004, *A&Ap*, 416, 1117
- Chevalier R. A., 1982, *ApJ*, 259, 302
- Chevalier R. A., 1998, *ApJ*, 499, 810
- Chiaki G., Yoshida N., Kitayama T., 2012, *ArXiv e-prints*, 1203.0820
- Clark P. C., Glover S. C. O., Smith R. J., Greif T. H., Klessen R. S., Bromm V., 2011, *Science*, 331, 1040
- Fomalont E. B., Kellermann K. I., Partridge R. B., Windhorst R. A., Richards E. A., 2002, *AJ*, 123, 2402
- Frebel A., Aoki W., Christlieb N., et al. 2005, *Nature*, 434, 871
- Furlanetto S. R., Loeb A., 2002, *ApJ*, 579, 1
- Gould R. J., 1975, *ApJ*, 196, 689
- Greif T. H., Bromm V., Clark P. C., Glover S. C. O., Smith R. J., Klessen R. S., Yoshida N., Springel V., 2012, *MNRAS*, 424, 399
- Greif T. H., Glover S. C. O., Bromm V., Klessen R. S., 2010, *ApJ*, 716, 510
- Greif T. H., Johnson J. L., Bromm V., Klessen R. S., 2007, *ApJ*, 670, 1
- Greif T. H., Johnson J. L., Klessen R. S., Bromm V., 2008, *MNRAS*, 387, 1021
- Greif T. H., Springel V., White S. D. M., Glover S. C. O., Clark P. C., Smith R. J., Klessen R. S., Bromm V., 2011, *ApJ*, 737, 75
- Hasegawa K., Umemura M., Susa H., 2009, *MNRAS*, 395, 1280
- Heavens A. F., Meisenheimer K., 1987, *MNRAS*, 225, 335
- Heger A., Woosley S. E., 2002, *ApJ*, 567, 532
- Hosokawa T., Omukai K., Yoshida N., Yorke H. W., 2011, *Science*, 334, 1250

- Hummel J. A., Pawlik A. H., Milosavljević M., Bromm V., 2012, *ApJ*, 755, 72
- Iliev I. T., Shapiro P. R., Ferrara A., Martel H., 2002, *ApJ*, 572, L123
- Iliev I. T., Shapiro P. R., Raga A. C., 2005, *MNRAS*, 361, 405
- Ioka K., Mészáros P., 2005, *ApJ*, 619, 684
- Iwamoto N., Umeda H., Tominaga N., Nomoto K., Maeda K., 2005, *Science*, 309, 451
- Joggerst C. C., Almgren A., Bell J., Heger A., Whalen D., Woosley S. E., 2010, *ApJ*, 709, 11
- Johnson J. L., Dalla Vecchia C., Khochfar S., 2012, *ArXiv e-prints*, 1206.5824
- Johnson J. L., Greif T. H., Bromm V., 2008, *MNRAS*, 388, 26
- Kitayama T., Yoshida N., 2005, *ApJ*, 630, 675
- Kitayama T., Yoshida N., Susa H., Umemura M., 2004, *ApJ*, 613, 631
- Komatsu E., Dunkley J., Nolta M. R., Bennett C. L., Gold B., Hinshaw G., Jarosik N., Larson D., Limon M., Page L., Spergel D. N., Halpern M., Hill R. S., Kogut A., Meyer S. S., Tucker G. S., Weiland J. L., Wollack E., Wright E. L., 2009, *ApJS*, 180, 330
- Koyama K., Petre R., Gotthelf E. V., Hwang U., Matsuura M., Ozaki M., Holt S. S., 1995, *Nature*, 378, 255
- Lai D. K., Bolte M., Johnson J. A., Lucatello S., Heger A., Woosley S. E., 2008, *ApJ*, 681, 1524
- Mackey J., Bromm V., Hernquist L., 2003, *ApJ*, 586, 1
- Malkov M. A., O’C Drury L., 2001, *Reports on Progress in Physics*, 64, 429
- Meiksin A., 2011, *MNRAS*, 417, 1480
- Moriya T. J., Blinnikov S. I., Tominaga N., Yoshida N., Tanaka M., Maeda K., Nomoto K., 2012, *ArXiv e-prints*, 1204.6109
- Muxlow T. W. B., Richards A. M. S., Garrington S. T., Wilkinson P. N., Anderson B., Richards E. A., Axon D. J., Fomalont E. B., Kellermann K. I., Partridge R. B., Windhorst R. A., 2005, *MNRAS*, 358, 1159
- Nagakura T., Hosokawa T., Omukai K., 2009, *MNRAS*, 399, 2183
- Nakamura F., Umemura M., 2001, *ApJ*, 548, 19
- Norris R. P., Afonso J., Bacon D., Beck R., Bell M., Beswick R. J., Best P., Bhatnagar S., Bonafede A., Brunetti G., Budavari T., Cassano R., Condo J. J., Cress C., Dabbech A., Feain I., 2012, *ArXiv e-prints*, 1210.7521
- Oh S. P., Cooray A., Kamionkowski M., 2003, *MNRAS*, 342, L20
- O’Shea B. W., Norman M. L., 2007, *ApJ*, 654, 66
- O’Shea B. W., Norman M. L., 2008, *ApJ*, 673, 14
- Owen F. N., Morrison G. E., 2008, *AJ*, 136, 1889
- Pan T., Kasen D., Loeb A., 2011, *ArXiv e-prints*, 1112.2710
- Reed D. S., Bower R., Frenk C. S., Jenkins A., Theuns T., 2007, *MNRAS*, 374, 2
- Rybicki G. B., Lightman A. P., 1986, *Radiative Processes in Astrophysics*. Wiley, 1986
- Scannapieco E., Madau P., Woosley S., Heger A., Ferrara A., 2005, *ApJ*, 633, 1031
- Schaerer D., 2002, *A&Ap*, 382, 28
- Scheuer P. A. G., Williams P. J. S., 1968, *ARA&A*, 6, 321
- Shapiro P. R., Ahn K., Alvarez M. A., Iliev I. T., Martel H., Ryu D., 2006, *ApJ*, 646, 681
- Shapiro P. R., Iliev I. T., Raga A. C., 2004, *MNRAS*, 348, 753
- Smith B. D., Sigurdsson S., 2007, *ApJ*, 661, L5
- Smith B. D., Turk M. J., Sigurdsson S., O’Shea B. W., Norman M. L., 2009, *ApJ*, 691, 441
- Soderberg A. M., Chevalier R. A., Kulkarni S. R., Frail D. A., 2006, *ApJ*, 651, 1005
- Stacy A., Greif T. H., Bromm V., 2010, *MNRAS*, 403, 45
- Stacy A., Greif T. H., Bromm V., 2011, *ArXiv e-prints*, 1109.3147
- Susa H., Umemura M., 2006, *ApJ*, 645, L93
- Susa H., Umemura M., Hasegawa K., 2009, *ApJ*, 702, 480
- Tanaka M., Moriya T. J., Yoshida N., Nomoto K., 2012, *MNRAS*, 422, 2675
- Turk M. J., Abel T., O’Shea B., 2009, *Science*, 325, 601
- Weiler K. W., Sramek R. A., Panagia N., van der Hulst J. M., Salvati M., 1986, *ApJ*, 301, 790
- Whalen D., Abel T., Norman M. L., 2004, *ApJ*, 610, 14
- Whalen D., Hueckstaedt R. M., McConkie T. O., 2010, *ApJ*, 712, 101
- Whalen D., O’Shea B. W., Smidt J., Norman M. L., 2008, *ApJ*, 679, 925
- Whalen D., van Veelen B., O’Shea B. W., Norman M. L., 2008, *ApJ*, 682, 49
- Whalen D. J., 2012, *The First Stars*, *Proceedings of Vulcano 2012: Frontiers in Astrophysics and Particle Physics*
- Whalen D. J., Joggerst C. C., Fryer C. L., Stiavelli M., Heger A., Holz D. E., 2012, *ArXiv e-prints*, 1209.5459
- Wise J. H., Abel T., 2007, *ApJ*, 671, 1559
- Wise J. H., Turk M. J., Norman M. L., Abel T., 2012, *ApJ*, 745, 50
- Woosley S. E., Blinnikov S., Heger A., 2007, *Nature*, 450, 390
- Yoshida N., Oh S. P., Kitayama T., Hernquist L., 2007, *ApJ*, 663, 687